

# NEAR-LIGHT COLOR PHOTOMETRIC STEREO FOR MONO-CHROMATICITY NON-LAMBERTIAN SURFACE

Zonglin Li<sup>1,†</sup>, Jieji Ren<sup>2,‡</sup>, Shuangfan Zhou<sup>1</sup>, Heng Guo<sup>1,\*</sup>,  
 Jinnuo Zhang<sup>2</sup>, Jiang Zhou<sup>2</sup>, Boxin Shi<sup>3</sup>, Zhanyu Ma<sup>1</sup>, Guoying Gu<sup>2</sup>

<sup>1</sup> Beijing University of Posts and Telecommunications, Beijing, China

<sup>2</sup> Shanghai Jiao Tong University, Shanghai, China

<sup>3</sup> Peking University, Beijing, China

## ABSTRACT

Color photometric stereo enables single-shot surface reconstruction, extending conventional photometric stereo that requires multiple images of a static scene under varying illumination to dynamic scenarios. However, most existing approaches assume ideal distant lighting and Lambertian reflectance, leaving more practical near-light conditions and non-Lambertian surfaces underexplored. To overcome this limitation, we propose a framework that leverages neural implicit representations for depth and BRDF modeling under the assumption of mono-chromaticity (uniform chromaticity and homogeneous material), which alleviates the inherent ill-posedness of color photometric stereo and allows for detailed surface recovery from just one image. Furthermore, we design a compact optical tactile sensor to validate our approach. Experiments on both synthetic and real-world datasets demonstrate that our method achieves accurate and robust surface reconstruction. To facilitate future research and ensure reproducibility, we have made our source code publicly available at <https://github.com/yulinjiaxue/near-light-color-ps>.

**Index Terms**— Near-Light Color Photometric Stereo, Neural Implicit Representation, Mono-Chromaticity,

## 1. INTRODUCTION

Recovering surface normals from images is a fundamental yet challenging computer vision task with broad applications in fields such as robotics and industrial inspection. Among various techniques developed to address this problem, Photometric Stereo (PS) has proven to be an effective approach. It estimates surface normals from intensity variations under different lighting conditions.

**Conventional methods**, initially proposed by Woodham [1], use least-squares optimization for static Lambertian surfaces and are constrained by distant illumination. Neural network-based approaches [2, 3] have improved performance on non-Lambertian objects. Under near-light illumination

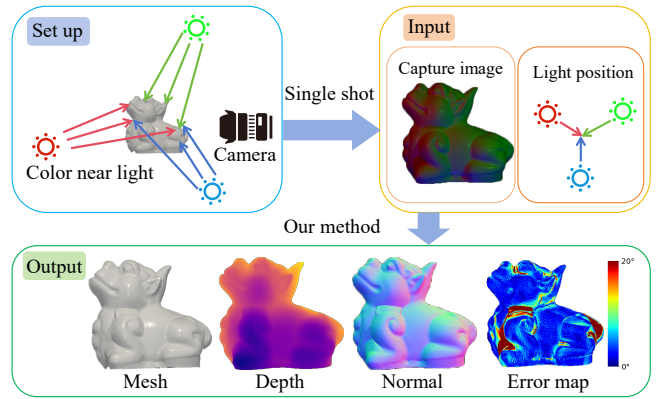


**Fig. 1.** Our method takes a single captured RGB image and the near-light source position as input, and outputs accurate surface normal, depth map and mesh.

setting, LEDPS [4] handles near-light conditions through alternating optimization. FastNFPS [5] has focused on non-Lambertian photometric stereo under uncalibrated near-field lighting. SDMUniPS [6] generalizes the setup to the case of general unknown lighting, enabling reconstruction under more general conditions. *However, conventional approaches necessitate capturing multiple images under varying illumination at different timestamps.*

**Color photometric stereo (CPS)** offers a single-shot alternative through spectral multiplexing, thereby enabling snapshot surface normal estimation. However, CPS is inherently ill-posed at the pixel level. This arises because, in CPS with  $k$  spectral light sources, each isolated pixel provides  $k$  observations, but each spectral band has its own distinct spectral reflectance, the total number of unknowns becomes  $k + 2$  ( $k$  spectral reflectances plus two surface normal parameters). To transform this ill-posed problem into a well-posed one, additional priors or constraints are typically required to regularize the solution. Anderson *et al.* [7] and Y. Ju *et al.* [8] employed prior information for simplification. Methods [9, 10] simplified the problem by assuming the surface spectral reflectance type to be gray or mono-chromatic with uniform albedo. Guo *et al.* [11] leveraged multiple pixels

<sup>†</sup> Equal contribution, <sup>\*</sup> Corresponding author: guoheng@bupt.edu.cn

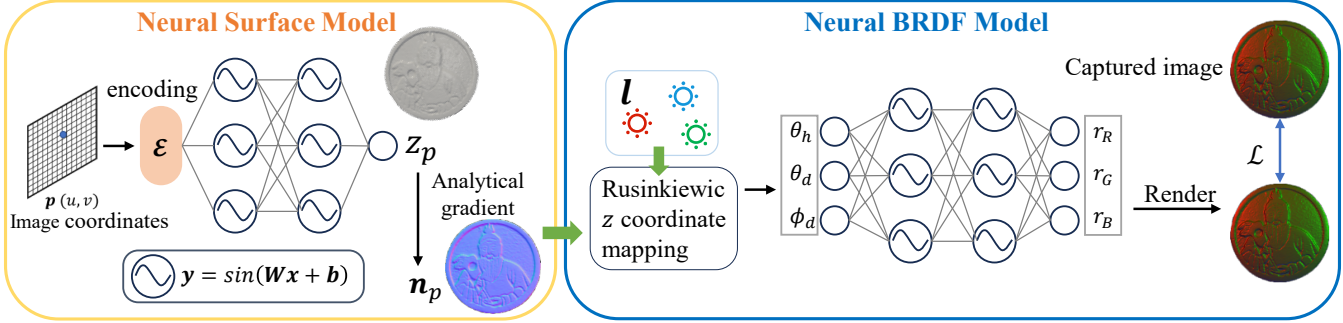


**Fig. 2.** Our method has a neural surface model and a neural BRDF model. The neural surface model estimates depth and normal from image coordinates, the BRDF model predicts reflectance using the angle between surface normal, light and view directions. The system is optimized via photometric consistency loss between the rendered and captured images.

sharing the same chromaticity  $\mathbf{v}$  to jointly constrain the solution under the assumption of mono-chromaticity. J. Lv *et al.* [12] addressed the non-Lambertian spectral BRDF under distant light by introducing a strong model assumption of Spectral Reflectance Decomposition, decomposing the BRDF into two simpler components. Physics-Free [13] achieves high-quality reconstruction of non-Lambertian surfaces even under uncalibrated distant illumination. The near-light photometric stereo method of Chen *et al.* [14] is only applicable to human faces under the Lambertian reflectance assumption. *The inherent ill-posedness of CPS is further exacerbated in practical near-light illumination setting and non-Lambertian reflectances.*

To address the ill-posedness of CPS under practical near-light illumination and non-Lambertian reflectance, we consider imposing mono-chromaticity prior, which assumes that the surface is uniform chromaticity and homogeneous material. This constraint has been shown to effectively regularize the reconstruction problem under such challenging conditions. Crucially, this assumption is not merely a modeling convenience—it is naturally satisfied in real-world sensing systems such as GelSight [15], which uses a homogeneous elastomer interface under fixed, near-field, single-shot illumination, precisely matching the mono-chromaticity prior. This makes it an ideal application for CPS under this constraint, and motivates the development of tailored photometric stereo methods with both theoretical and practical value.

Under the assumption of mono-chromaticity, we propose a neural implicit modeling framework for near-light CPS and design a practical capture setup, as shown in Fig. 1. We model the surface depth using the differentiable neural representation, which enables the simultaneous optimization of both depth and normal, thereby reducing the difficulty of surface shape estimation. Simultaneously, under the homogeneous material constraint, the surface reflectance exhibits a unified BRDF structure across the entire surface. This constraint allows the BRDF to be effectively represented using a single implicit neural network. Further incorporating the uniform chromaticity condition, the solution of non-Lambertian spectral BRDF becomes tractable. This approach facilitates

accurate normal estimation and robust geometry reconstruction under near-light conditions. We also designed a compact near-light visuo-tactile sensor (NearLightTactile) sensor for qualitative evaluation of our method’s performance in real-world scenarios.

Our contributions can be summarized as follows:

- We propose the first near-light CPS method, allowing accurate normal recovery for non-Lambertian surface under practical near light setting;
- We propose to use a neural surface model to jointly recover depth and normal, and a neural BRDF model for mono-chromaticity BRDF, formulating the near-light CPS to be well-posed;
- We design a tactile sensor **NearLightTactile**, validating our method in tactile-based shape reconstruction.

## 2. METHOD

Our self-supervised framework recovers high-fidelity surface normals from a single RGB image under known near-light illumination, without ground-truth data or complex calibration. We jointly optimize a neural surface and a neural BRDF model through photometric consistency loss between the rendered and input, without requiring ground-truth normals. The overall architecture is shown in Fig. 2.

### 2.1. Neural Surface Model

Instead of directly predicting surface normals, we estimate per-pixel depth values and subsequently derive normals analytically, thereby resolving the ill-posedness arising from geometric coupling in near-light CPS.

Given a pixel coordinate  $\mathbf{p} = (u, v)^\top \in \mathbb{R}^2$ , we first embed it using a multi-resolution hash encoding  $\mathcal{E}(\cdot)$  [16], which preserves high-frequency spatial details. The encoded feature is then mapped to a scalar depth value  $z$  via a sinusoidal MLP (SIREN [17]):

$$z = f^{\text{SURFACE}}(\mathcal{E}(\mathbf{p}); \theta_s), \quad (1)$$

where  $\theta_s$  denotes the learnable parameters. The surface normal  $\mathbf{n}$  is subsequently derived from the spatial gradient of the depth map  $\nabla z = (\partial z / \partial u, \partial z / \partial v)^\top$  using the perspective camera model [18]:

$$\mathbf{n} = \eta \left( \begin{bmatrix} f \nabla z \\ -z - \nabla z^\top \mathbf{p} \end{bmatrix} \right), \quad (2)$$

where  $\eta(\cdot)$  denotes  $\ell_2$  normalization.

## 2.2. Neural BRDF Model

With geometry (depth and normals) recovered from the first module, we further model spatially-varying reflectance following [19]. For a surface point  $\mathbf{x}$  with normal  $\mathbf{n}$  and a near-light source at position  $\mathbf{l}$ , the normalized incident light direction is  $\mathbf{q} = \eta(\mathbf{l} - \mathbf{x})$ . The pair  $(\mathbf{q}, \mathbf{n})$  is then transformed into the Rusinkiewicz parameterization  $(\theta_h, \theta_d, \phi_d)$  [20]. We learn the mapping from  $(\theta_h, \theta_d, \phi_d)$  to the reflectance  $\mathbf{r}$  using an implicit neural BRDF model:

$$\mathbf{r} = f^{\text{BRDF}}((\theta_h, \theta_d, \phi_d); \theta_r), \quad (3)$$

where  $\theta_r$  denotes the learnable parameters. To capture wavelength-dependent reflectance under colored LED illumination, we employ independent MLP branches for the RGB channels and concatenate their outputs as  $\mathbf{r} = [r_R, r_G, r_B]$ .

## 2.3. Differentiable Rendering and Optimization

The learning process is guided by a reconstruction loss that compares the input image with a rendered image synthesized from the estimated geometry and reflectance. The RGB value  $\hat{I}_{u,v}$  at pixel  $(u, v)$  is computed using a near-light image formation model:

$$\hat{I}_{u,v} = \mathbf{r} \cdot \frac{\varphi}{\|\mathbf{l} - \mathbf{x}\|^2} \max(\mathbf{q}^\top \mathbf{n}, 0), \quad (4)$$

where  $\varphi$  denotes the light intensity, set to 1 in our implementation. This image formation model accounts for both light attenuation ( $1/\|\mathbf{l} - \mathbf{x}\|^2$ ) and cosine falloff ( $\max(\mathbf{q}^\top \mathbf{n}, 0)$ ).

The network is trained end-to-end by minimizing an  $\ell_1$  reconstruction loss:

$$\mathcal{L} = \sum_{u,v} \|I_{u,v} - \hat{I}_{u,v}\|_1. \quad (5)$$

## 3. EXPERIMENTS

### 3.1. Experimental Setup

Due to the lack of publicly available CPS datasets captured under near-light conditions, we generate a synthetic dataset of five objects using Blender v3.6.<sup>1</sup>, designed to cover variations in color, reflectance, and geometry. Our dataset comprises both white and colored objects to examine robustness against intrinsic color; Lambertian and non-Lambertian materials (e.g., metal, ceramic) to test reflectance modeling; and objects ranging from flat to curved and rugged surfaces to evaluate reconstruction across different geometric complexities. All objects are rendered with Blender’s principled BSDF shader. The camera is positioned 35 mm away from the object, with a sensor size of  $2.3 \times 1.44$  mm, focal length of 2.8 mm, and image resolution of  $640 \times 480$ . A point light

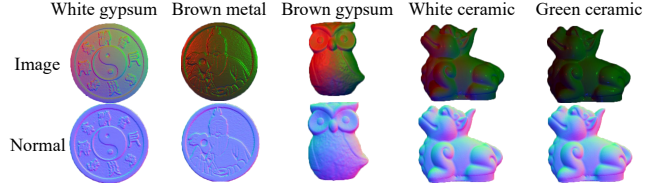


**Fig. 3.** Synthetic dataset covering varying geometric details and reflection types.

**Table 1.** Quantitative comparison of surface normals

Object	Mean Angular Error(°) ↓				
	Ours	LSPS [1]	LEDPS [4]	RGBPS [9]	FastNFPS [5]
White gypsum	<b>2.54</b>	17.98	3.55	17.91	25.64
Brown metal	<b>4.74</b>	24.67	13.11	20.41	21.19
Brown gypsum	<b>2.43</b>	13.84	6.41	13.98	12.04
White ceramic	<b>6.38</b>	17.96	11.89	18.50	18.48
Green ceramic	<b>5.57</b>	17.82	11.77	18.14	18.10

source is placed 11 mm away from the camera longitudinally and 21.5 mm laterally. Three colored LEDs (red, green, blue) are simulated to provide near-light illumination, and their intensity is tuned to avoid over-exposure. Rendering is performed in Blender Cycles using a linear color space to preserve radiometric consistency.

Since most CPS methods require constraints from four or more light sources, we ultimately opted to compare our method with LSPS [1], LEDPS [4], RGB-PS [9] and FastNFPS [5], using their default implementations where available. Performance is evaluated with the standard Mean Angular Error (MAE) in degrees between predicted and ground-truth normals.

### 3.2. Experiment Results and Analysis

Quantitative results are summarized in Table 1 and three qualitative results are illustrated in Fig. 4. Our method consistently produces reconstructions that are visually closest to the ground truth, accurately preserving fine geometric details. The distant-light methods LSPS [1] and RGBPS [9] are not suitable for near-light conditions, resulting in poor reconstruction performance. LEDPS [4], on the other hand, performs poorly when dealing with non-Lambertian objects. FastNFPS [5] method does not perform well on our three-light, sub-millimeter-scale dataset. We attribute this degradation to two main factors: (1) its lighting calibration network is unstable under near-light conditions with very few sources, resulting in inaccurate light estimation; (2) its training data does not cover such lighting-to-object scale ratios, which restricts generalization. This underscores the significant challenges inherent in near-light reconstruction for sub-millimeter-scale scenarios.

The quantitative results on the synthetic dataset demonstrate that our method reformulates the originally ill-posed problem of CPS under near-light illumination into a well-posed one. This is achieved by implicitly disentangling geometry through neural representations while decoupling non-Lambertian spectral BRDF using mono-chromaticity

<sup>1</sup><https://www.blender.org/>

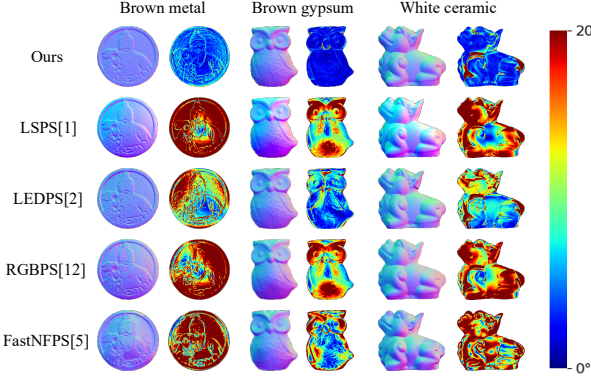


**Fig. 4.** Quantitative comparison of surface normal.

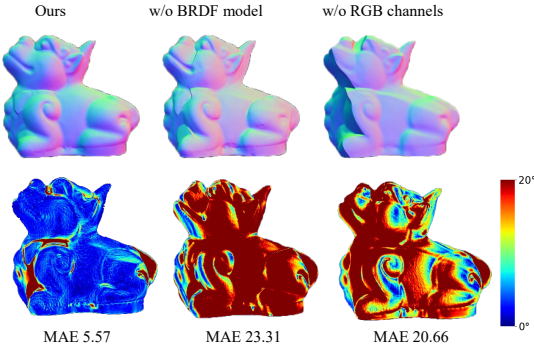


**Fig. 5.** Ablation Study of our method.

constraints and an implicit BRDF formulation. Through this two-fold decoupling, we show improved reconstruction accuracy under challenging near-light conditions.

### 3.3. Ablation Study

We perform two ablation studies on the neural BRDF model to validate our design choices, with results shown in Fig. 5. (1) w/o BRDF model: Replacing the neural BRDF with a least-squares estimated albedo leads to a substantial performance drop, highlighting the importance of explicitly modeling non-Lambertian reflectance. (2) w/o RGB channels: Predicting a single output for all color channels instead of three independent ones also degrades performance, demonstrating that wavelength-dependent reflectance modeling is essential under colored lighting.

### 3.4. Real-World Validation

As detailed in Fig. 6, this sensor provides a challenging real-world testbed characterized by near-light illumination, single imaging and sub-millimeter geometric features.

#### 3.4.1. Robustness against Crosstalk

Crosstalk [21] poses a major challenge for CPS in compact systems, due to spectral overlap in RGB filters and pixel-level cross-coupling in miniaturized sensors. This violates the channel independence assumption in RGB-PS and causes significant artifacts.

To overcome Crosstalk, we propose a lightweight data-driven Crosstalk Correction Module (CCM) that models crosstalk as a pixel-wise mapping  $\mathcal{T}$  from  $\mathbf{I}_{\text{obs}}$  to  $\mathbf{I}_{\text{ideal}}$ .

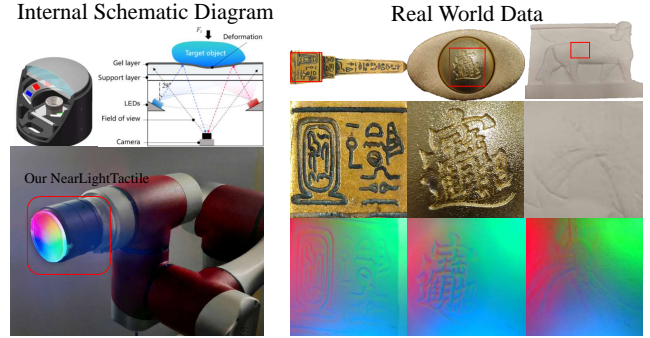


**Fig. 6.** Real-world validation uses our custom vision-based tactile sensor, shown alongside sample captured images.

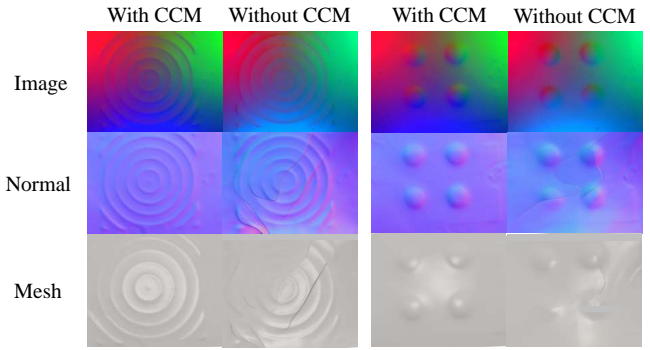


**Fig. 7.** Results after and before using the CCM.

Using baseline images  $\mathbf{I}_R, \mathbf{I}_G, \mathbf{I}_B$  captured under separate monochromatic LEDs, we use a compact MLP to learn  $\mathcal{T}$ , which serves as a pre-processing step to restore photometric consistency before normal estimation.

#### 3.4.2. Qualitative Results on Real-World Data

We evaluate our complete system (sensor + CCM + method) by pressing objects with fine, sub-millimeter textures against the elastomer layer. Fig. 7 shows the results for two objects. After crosstalk correction, input images exhibit improved channel separation. Our method reconstructs high-quality normals and detailed 3D geometry. The successful deployment and validation of our *NearLightTactile* demonstrates the potential practical utility of the proposed approach. By mitigating crosstalk through targeted calibration, the method achieves normal reconstruction,

## 4. CONCLUSION

In this paper, we presented the first non-Lambertian CPS method under near-light conditions. By introducing a neural surface model to jointly constrain surface normals and depth, together with a neural BRDF model that enforces a mono-chromaticity constraint, our approach reduces reconstruction ambiguity and makes CPS tractable. The proposed framework achieves accurate shape recovery from a single multispectral snapshot and demonstrates practical feasibility through real-world validation with a compact visuo-tactile sensor.

## 5. ACKNOWLEDGEMENTS

This work was supported by Beijing-Tianjin-Hebei Basic Research Funding Program No. F2024502017, the National Natural Science Foundation of China (Grant No. 62472044, U24B20155, U23B2052, and 52505029), Hebei Natural Science Foundation Project No. 242Q0101Z, Beijing Municipal Science & Technology Program No. Z251100007125021, and Science and Technology Commission of Shanghai Municipality No. 25ZR1401191.

## 6. REFERENCES

- [1] R. J. Woodham, “Photometric method for determining surface orientation from multiple images,” *Optical Engineering*, vol. 19, no. 1, pp. 139–144, January 1980.
- [2] S. Ikehata, “Cnn-ps: Cnn-based photometric stereo for general non-convex surfaces,” in *Proceedings of the European Conference on Computer Vision (ECCV)*, 2018, pp. 3–18.
- [3] G. Chen, K. Han, B. Shi, et al., “Deep photometric stereo for non-lambertian surfaces,” *IEEE Transactions on Pattern Analysis and Machine Intelligence*, vol. 44, no. 1, pp. 129–142, 2020.
- [4] Y. Quéau, B. Durix, T. Wu, et al., “Led-based photometric stereo: Modeling, calibration and numerical solution,” *Journal of Mathematical Imaging and Vision*, vol. 60, pp. 313–340, 2018.
- [5] D. Lichy, S. Sengupta, and D. W. Jacobs, “Fast light-weight near-field photometric stereo,” in *Proceedings of the IEEE/CVF Conference on Computer Vision and Pattern Recognition*, 2022, pp. 12612–12621.
- [6] S. Ikehata, “Scalable, detailed and mask-free universal photometric stereo,” in *Proceedings of the IEEE/CVF Conference on Computer Vision and Pattern Recognition*, 2023, pp. 13198–13207.
- [7] R. Anderson, B. Stenger, and R. Cipolla, “Augmenting depth camera output using photometric stereo,” *Machine Vision and Applications*, 2011.
- [8] Y. Ju, X. Dong, Y. Wang, L. Qi, and J. Dong, “A dual- cue network for multispectral photometric stereo,” *Pattern Recognition*, p. 107162, 2020.
- [9] A. Chakrabarti and K. Sunkavalli, “Single-image RGB photometric stereo with spatially-varying albedo,” in *2016 Fourth International Conference on 3D Vision (3DV)*. 2016, pp. 258–266, IEEE.
- [10] K. Ozawa, I. Sato, and M. Yamaguchi, “Single color image photometric stereo for multi-colored surfaces,” *Computer Vision and Image Understanding*, pp. 140–149, 2018.
- [11] H. Guo, F. Okura, B. Shi, T. Funatomi, Y. Mukaigawa, and Y. Matsushita, “Multispectral photometric stereo for spatially-varying spectral reflectances: A well posed problem?,” in *Proc. of Computer Vision and Pattern Recognition*, 2021, pp. 963–971.
- [12] J. Lv, H. Guo, G. Chen, et al., “Non-lambertian multispectral photometric stereo via spectral reflectance decomposition,” in *Proceedings of the International Joint Conference on Artificial Intelligence (IJCAI)*, 2023, pp. 1249–1257.
- [13] S. Ikehata and Y. Asano, “Physics-free spectrally multiplexed photometric stereo under unknown spectral composition,” in *Proceedings of the European Conference on Computer Vision (ECCV)*, 2024, pp. 295–312.
- [14] Z. Chen, Y. Ji, M. Zhou, et al., “3D face reconstruction using color photometric stereo with uncalibrated near point lights,” in *Proc. of International Conference on Computational Photography*. 2020, pp. 1–12, IEEE.
- [15] W. Yuan, S. Dong, and E. H. Adelson, “GelSight: High-resolution robot tactile sensors for estimating geometry and force,” *Sensors*, vol. 17, no. 12, pp. 2762, 2017.
- [16] T. Müller, A. Evans, C. Schied, et al., “Instant neural graphics primitives with a multiresolution hash encoding,” *ACM Transactions on Graphics (TOG)*, vol. 41, no. 4, pp. 1–15, 2022.
- [17] V. Sitzmann, J. Martel, A. Bergman, et al., “Implicit neural representations with periodic activation functions,” *Advances in Neural Information Processing Systems*, vol. 33, pp. 7462–7473, 2020.
- [18] Y. Quéau, J. D. Durou, and J. F. Aujol, “Normal integration: A survey,” *Journal of Mathematical Imaging and Vision*, vol. 60, pp. 576–593, 2018.
- [19] H. Guo, B. Shi, and Y. Matsushita, “Neural BRDF plugin for unsupervised photometric stereo,” in *2023 8th IEEE International Conference on Network Intelligence and Digital Content (IC-NIDC)*. 2023, pp. 137–141, IEEE.
- [20] S. M. Rusinkiewicz, “A new change of variables for efficient BRDF representation,” in *Rendering Techniques’98: Proceedings of the Eurographics Workshop in Vienna, Austria, June 29–July 1, 1998*. 1998, 9, pp. 11–22, Springer Vienna.
- [21] A. Ahmad, A. Kumar, V. Dubey, et al., “Characterization of color cross-talk of CCD detectors and its influence in multispectral quantitative phase imaging,” *Optics Express*, vol. 27, no. 4, pp. 4572–4589, 2019.